EDGE ARTICLE

Mechanically tunable porous gels constructed *via* the dual coordination/covalent polymerization of coumarin-functionalized rhodium–organic cuboctahedra†

David W. Burke,*[a] Masataka Yamashita,[b] Zaoming Wang, [ID] [a] Mako Kuzumoto,[b] Kenji Urayama, [ID] [b] Kei Saito [ID] [c] and Shuhei Furukawa [ID] *[ad]

Polymer-based soft materials constructed from defined molecular pores, such as metal–organic polyhedra (MOPs), promise to merge the outstanding and diverse mechanical properties of conventional nonporous polymers with atomically-precise molecular recognition capabilities. Thus far, soft MOP networks have been constructed primarily using rigid, labile coordination bonds or dynamic covalent bonds, providing static networks without intrinsic mechanisms to optimize their response to mechanical stimuli. Here, we report the construction of flexible, doubly crosslinked MOP gels *via* mutually compatible coordination and covalent polymerization techniques. Our method employs dirhodium paddlewheel-based MOPs bearing both open metal sites, which enable their coordination-driven assembly, and photodimerizable coumarin side chains for covalent polymerization (Coumarin-RhMOPs). Incubation of Coumarin-RhMOPs with ditopic linkers enabled their coordination-driven polymerization into porous colloidal gels. Site-selective irradiation of coordination-linked Coumarin-RhMOP gels afforded doubly crosslinked gels with improved strain tolerance and higher stiffness. Selective dissociation of coordination-crosslinkers provided highly deformable covalent Coumarin-RhMOP gels. The postsynthetic addition of ditopic ligands to covalent gels enabled the reversible modulation of their mechanical properties. These findings highlight the possibility of incorporating multiple responsive crosslinks in porous MOP networks to rationally tune their responses to mechanical stress, paving the way to their practical implementation as next-generation chemical separators, catalysts, and drug delivery vehicles.

Introduction

Polymer-based soft materials, such as thin films, foams, and gels, are ubiquitous in modern society due to their ability to deform rather than fracture under mechanical stress, a feature which makes them ideal for implementation as chemical separation membranes,[1] flexible electronics,[2] biomedical implants,[3] and more.[4,5] To optimize a polymer network's performance and longevity in each of these applications, achieving fine control of its mechanical properties, including

hardness, strength, and toughness, is of paramount importance.[6–8] For example, a polymer hydrogel employed as a scaffold for engineered tissue must mimic the elastic deformability of the corresponding biological tissue while maintaining its integrity under high compressive, tensile, and shear stresses associated with bodily motion.[6,8,9] Likewise, a polymer membrane implemented into a liquid-phase chemical separation process must be sufficiently flexible to wrap into an industrial filtration module while resisting irreversible deformation, fracture, or pore collapse under extended operation at elevated transmembrane pressures.[7,10] These examples outline the importance of incorporating designed stress responses into soft materials, and motivate the development of polymerization strategies that afford functional materials with controlled deformability, fracture resistance, and strain tolerance.

Structurally programmable molecular cages, such as metal–organic polyhedra (MOPs),[11,12] have garnered recent attention as building blocks for soft materials because their symmetric surfaces can provide a high density of anchor points for cross-linkers, and their intrinsic cavities can imbue materials with

[a] *Institute for Integrated Cell-Material Sciences (WPI-iCeMS), Kyoto University, Yoshida, Sakyo-ku, Kyoto 606-8501, Japan. E-mail: davburke@hiroshima-u.ac.jp; shuhei.furukawa@icems.kyoto-u.ac.jp*

[b] *Department of Material Chemistry, Graduate School of Engineering, Kyoto University, Katsura, Nishikyo-ku, Kyoto 615-8510, Japan*

[c] *Graduate School of Advanced Integrated Studies in Human Survivability (GSAIS), Kyoto University, Sakyo-ku, Kyoto 606-8306, Japan*

[d] *Department of Synthetic Chemistry and Biological Chemistry, Graduate School of Engineering, Kyoto University, Katsura, Nishikyo-ku, Kyoto 615-8510, Japan*

† Electronic supplementary information (ESI) available. See DOI: https://doi.org/10.1039/d5sc00535c

selective molecular recognition and transport capabilities.[13–15] Such porous soft materials are of interest for use in applications where controlled molecular transport or release must be paired with deformability and fracture resistance, such as pressure-driven chemical separations and drug delivery.[16–19] Thus far, MOP polymerization protocols have relied on either the covalent condensation of reactive functional groups on the cage surface with compatible comonomers,[20–27] or the coordination of their open metal sites with multitopic ligands.[14,28–34] In nearly all reported cases, the polymerization events afforded static polymer networks, with compositions and mechanical properties that could not be adjusted without decomposing the network into its constituent building units (Fig. 1).

Towards dynamic MOP networks with tunable mechanical properties, Johnson and coworkers reported the co-assembly of photoswitchable polymer ligands (L) with Pd^{2+} to produce polymer networks crosslinked by Pd_3L_6 rings.[35] Photo-irradiation of the polymer ligands facilitated their reversible interconversion between ring-open and ring-closed isomers, resulting in the restructuring of the Pd-organic crosslinks between Pd_3L_6 rings and $Pd_{24}L_{48}$ rhombicuboctahedra. This structural reorganization resulted in a reversible 2-fold change in the shear storage modulus (G') of the gel.[35] To our knowledge, this study remains the only example of mechanical modulation in a dynamic polymer network based on metal–organic cages (Fig. 1). While several strategies have emerged to control the deformability and fracture resistance of nonporous soft materials, such as including two polymer networks with contrasting mechanical properties (brittle and malleable) in a single

material,[8,36,37] or incorporating multiple responsive crosslinking chemistries into one material,[38,39] these strategies have not yet been explored in the context of MOP-based polymers. Given that MOPs can be connected both through coordination and covalent approaches, we envisioned that the simultaneous inclusion of reversible coordination and covalent crosslinks with divergent mechanical properties might provide a new approach to finely tune the stress responses of elastic MOP networks (Fig. 1).

Herein, we report the stepwise polymerization of dual crosslinked MOP networks through orthogonal coordination and covalent approaches (Fig. 2). First, we prepared discrete dirhodium paddlewheel-based MOPs covalently decorated with flexible, coumarin-terminated alkyl side chains (Coumarin-RhMOPs). The open metal sites of RhMOPs enable their direct polymerization into hierarchically porous colloidal gels in the presence of rigid, ditopic N-donor ligands.[29] Meanwhile, the coumarin side chains undergo [2 + 2] cycloaddition reactions when exposed to UV light to produce cyclobutane-based dimers,[40] facilitating the photopolymerization of the cages. By organizing Coumarin-RhMOPs into gels through coordination polymerization techniques, then irradiating with UV light to form cyclobutane crosslinks, doubly crosslinked Coumarin-RhMOP gels were prepared, which exhibited a higher shear storage modulus ($G' = 116$ Pa), and tolerated greater strain ($\gamma = 63\%$) than their solely coordination-linked counterparts ($G' = 64$ Pa, $\gamma = 25\%$). Treatment of the dual network with acid promoted the reversible dissociation of the coordination crosslinkers, providing solely covalent Coumarin-RhMOP gels with exceptional deformability ($G' = 12$ Pa, $\gamma = 101\%$) due to the
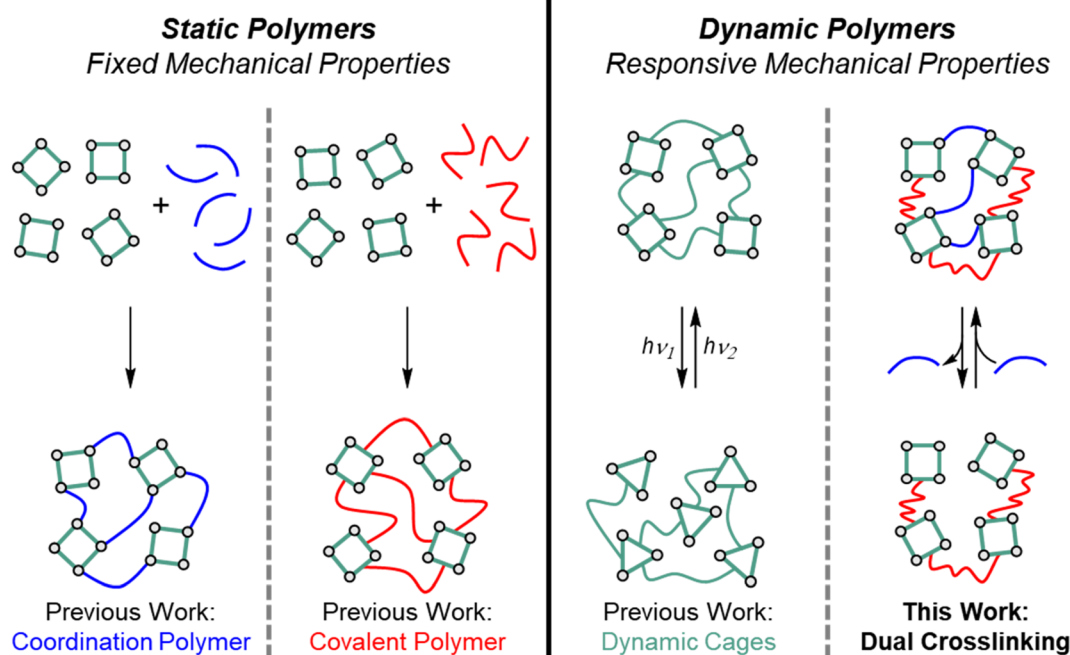

Fig. 1 Overview of existing MOP polymerization methods. Previous studies have primarily explored the coordination and covalent polymerization of MOPs into static polymer networks with fixed mechanical properties. Johnson and coworkers demonstrated the preparation of gel networks with photoreversible mechanical properties based on the light-induced restructuring of Pd–organic cages.[35] In this work, we adopt a new approach to synthesize mechanically tunable MOP networks by incorporating two crosslinkers with orthogonal stimuli responses.
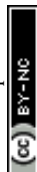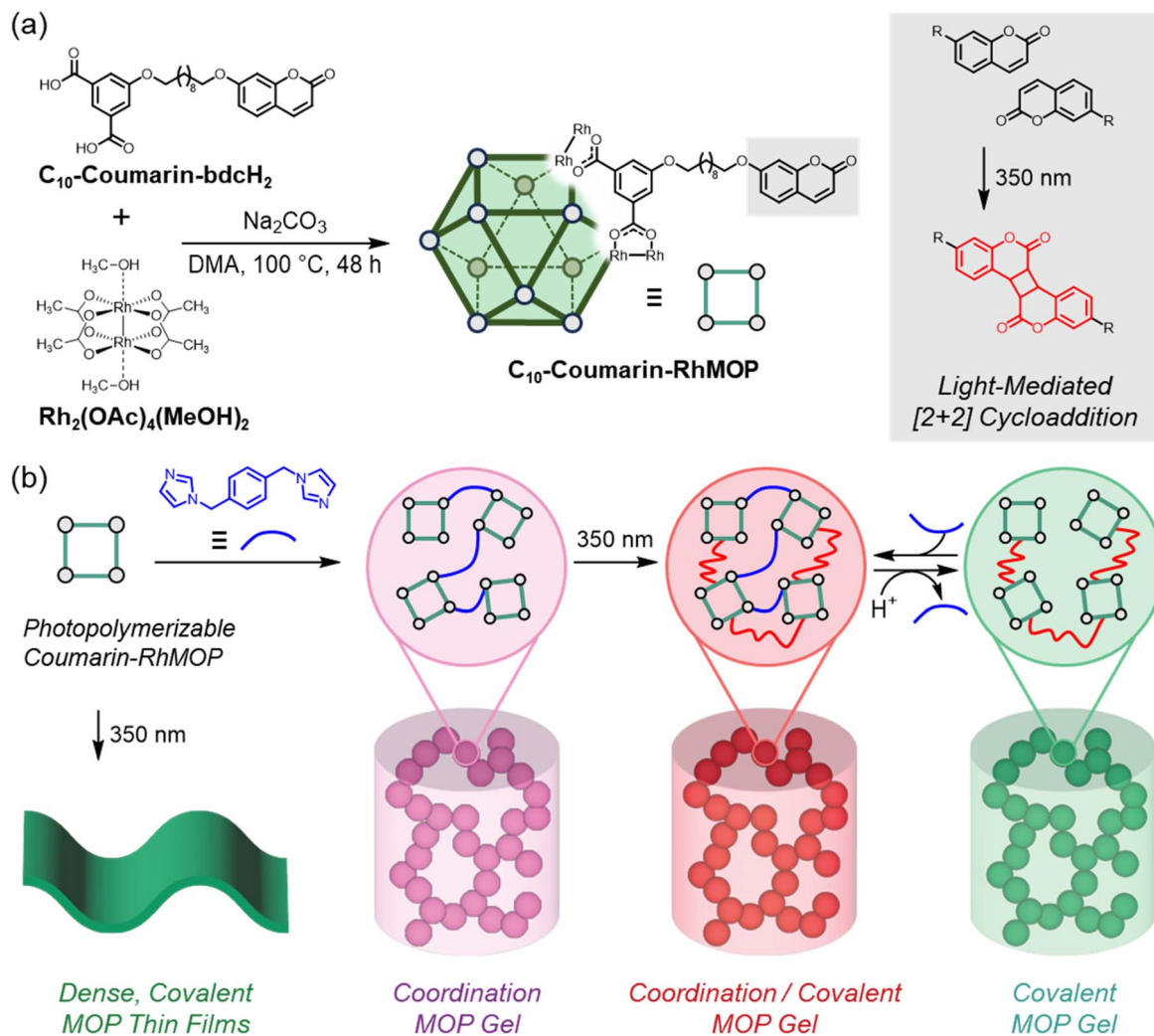
Fig. 2 (a) Bottom-up synthesis of C_{10}-Coumarin-RhMOP from a coumarin-functionalized isophthalic acid monomer (C_{10}-Coumarin-bdcH$_2$) and Rh$_2$(OAc)$_4$(MeOH)$_2$. The coumarin side chains undergo [2 + 2] cycloaddition reactions when irradiated at 350 nm, resulting in the formation of cyclobutane-based dimers. (b) Overview of the preparation of soft materials from the C_{10}-Coumarin-RhMOP via orthogonal covalent/coordination polymerization techniques. Direct irradiation of high-concentration MOP solutions affords dense, photopolymerized thin films. Alternatively, ditopic imidazole-mediated coordination polymerization provides hierarchically porous MOP gels (purple), which undergo subsequent photocrosslinking under UV light to form dual coordination/covalent networks (red). Dissociation of the coordination crosslinker with acid provides covalent MOP gels connected entirely through cyclobutane crosslinks. Addition and dissociation of ditopic imidazoles facilitates the reversible interconversion of covalent and coordination/covalent networks, thus modulating their mechanical properties.

flexible alkyl chains bridging the coumarin residues to the MOP surface. Readdition of the rigid coordination crosslinkers led to a near-complete recovery of the mechanical properties of the doubly crosslinked gel, highlighting an opportunity to reversibly modulate the gel stiffness through the dual crosslinking approach. Moreover, the hierarchical porosity of the initial coordination gel was fully maintained throughout the photopolymerization and crosslinker dissociation processes. These results highlight the promise of combining coordination and covalent polymerization techniques to assemble molecular pores into robust, mechanically tunable porous networks, opening up new possibilities for this emergent class of materials.

Results and discussion

Design of Coumarin-RhMOPs

Among representative MOPs, dirhodium paddlewheel-based metal–organic cuboctahedra (RhMOPs) with the composition of $[Rh_2(bdc)_2]_{12}$ (bdc = isophthalate derivatives) are attractive candidates for building doubly crosslinked networks, since their isophthalate backbone and open metal sites can serve as connection points for covalent and coordination crosslinkers, respectively.[41] Another key advantage of RhMOPs is that the cages are diamagnetic, enabling their facile structural characterization by nuclear magnetic resonance (NMR) spectroscopy techniques.[42] The coordination-driven polymerization of RhMOPs in the presence of rigid ditopic imidazole linkers is

well-established, and typically affords hierarchically porous colloidal gels, which can be activated to the corresponding aerogels ($S_{BET} \approx$ 100–600 m^2 g^{-1}) via treatment with super-critical CO_2.[14,28,29,31,33]

We envisioned that the incorporation of flexible, polymerizable side chains onto the RhMOP surface could facilitate their dual coordination/covalent assembly, where the presence of rigid and flexible crosslinkers would afford both deformation resistance and elevated strain tolerance. Among covalent polymerization chemistries, light-mediated [2 + 2] cycloaddition reactions between alkene derivatives, such as coumarin, are particularly appealing, as they can be triggered in the absence of photoinitiators and comonomers, and the resulting cyclobutane linkages are chemically robust.[40,43–46] Moreover, the use of light as a stimulus could provide spatiotemporal control over MOP assembly. To our knowledge, only two publications have reported MOPs bearing side chains suitable for [2 + 2] cycloaddition-based polymerization.[47,48] The first study, by Park and coworkers, investigated the benzophenone-mediated photoreduction of coumarin-functionalized Cu-paddlewheel MOPs, where the coumarin side chains acted as triplet quenchers of excited benzophenone, thus modulating the rate of photoreduction.[47] In a follow-up study, Johnson and coworkers leveraged the same Cu-paddlewheel MOPs as crosslinks in polymer gels, which disassembled upon benzophenone-mediated photoreduction, providing the corresponding polymer sols.[48] Neither study discussed the potential for coumarin dimerization under UV irradiation, nor rigorously examined the photochemistry of the MOPs in the absence of benzophenone. Given the superior oxidative stability of RhMOPs, we envisioned that the incorporation of coumarin side chains onto their surfaces could afford molecular pores suitable for site-selective photopolymerization into flexible porous networks via inter-cage cycloaddition reactions.

Synthesis and solution-state photochemistry of Coumarin-RhMOPs

Coumarin-RhMOPs were synthesized via solvothermal condensation reactions between coumarin-functionalized isophthalic acids and dirhodium acetates, as verified by NMR spectroscopy, UV-Vis spectroscopy, and mass spectrometry measurements. To incorporate coumarin functionality onto the surfaces of RhMOPs while preserving their axial coordination sites, we designed a coumarin-tethered isophthalic acid (C_{10}-**Coumarin-bdcH$_2$**) with a decyl chain to bridge the isophthalic acid and coumarin residues to endow the coumarin with sufficient flexibility to adopt the intermolecular arrangements required for [2 + 2] cycloaddition reactions (see ESI Section 2.1† for complete synthetic protocol).[49]

Incubation of C_{10}-**Coumarin-bdcH$_2$** with dirhodium acetates in N,N-dimethylacetamide (DMA) at 100 °C afforded the targeted cuboctahedral MOP (C_{10}-**Coumarin-RhMOP**, composed of [Rh$_2$(C_{10}-Coumarin-bdc)$_2$]$_{12}$) as a blue-green powder (Fig. 2a), which was washed with aqueous NaOH and H$_2$O to remove unreacted starting materials prior to solvent exchange and vacuum activation (see ESI Section 2.2.1† for complete synthetic protocol).

To confirm the formation of the targeted cage, the powder was first analyzed by ^{1}H and ^{13}C NMR spectroscopies and ^{1}H diffusion-ordered spectroscopy (DOSY) in DMF-d_7. Both ^{1}H and ^{13}C NMR spectra of the cage exhibit peaks matching the relative positions, splitting patterns, and integrations of the C_{10}-**Coumarin-bdcH$_2$** monomer, but with notable broadening of the isophthalate signals nearest to the carboxylate residues, consistent with coordination to the dirhodium paddlewheel motif (Fig. S1 and S2†). DOSY revealed a consistent diffusion coefficient ($D = 7.53 \times 10^{-11}$ m^2 s^{-1}) for all peaks, corresponding to a hydrodynamic radius of 3.6 nm, which is in close agreement with a model of the targeted cage ($R = 3.4$ nm, Fig. S3 and S4†).

To verify that the synthesized complex is composed of 12 dirhodium paddlewheel units, as expected for cuboctahedral RhMOPs, a dimethylformamide (DMF) solution of C_{10}-**Coumarin-RhMOP** was titrated with an N-donor ligand capable of coordinating to the dirhodium paddlewheel, 1-dodecylimidazole (diz), and the associated visible absorption changes were assessed by UV-Vis spectroscopy (Fig. S5†). A gradual, stepwise shift in the $\pi^* \rightarrow \sigma^*$ band of the dirhodium paddlewheel from $\lambda_{max} = 594$ nm to 561 nm was observed as up to 12 stoichiometric equivalents of ligand were added, consistent with the coordination of imidazole moieties to the 12 exohedral open metal sites of a cuboctahedral cage. Further addition of diz up to 24 total equivalents produced negligible change in λ_{max}, suggesting that this ligand is unable to pass through the narrow pore window of the cuboctahedron and coordinate to the endohedral open metal sites. This result matches our previous study.[29]

Matrix-assisted laser desorption ionization (MALDI) mass spectrometry was leveraged to verify the expected mass of the cage (Fig. S6†), revealing a peak at $m/z = 14\,039$, which is consistent with the [M + Na] ion of the C_{10}-**Coumarin-RhMOP** (expected: $m/z = 14\,025$). Note that the mass spectrum contains several additional peaks in the range of $m/z = 13\,000–14000$, which were not readily assignable to the predicted MOP structure. Given the strong absorption of the coumarin side chains at $\lambda < 370$ nm, we expect that these lower m/z peaks may be attributable to the partial decomposition of the MOP upon irradiation with the 337 nm nitrogen gas laser during ionization. Collectively, these results strongly support the formation of the cuboctahedral C_{10}-**Coumarin-RhMOP**.

To identify suitable reaction conditions to promote the photochemical dimerization of RhMOP-bound coumarins, we first explored the dimerization of free C_{10}-**Coumarin-bdcH$_2$** in solution. A 20 mM solution of C_{10}-**Coumarin-bdcH$_2$** in DMSO-d_6 was placed in a UV photoreactor ($\lambda_{max} = 350$ nm, irradiance = 4 mW cm^{-2}) and irradiated for 72 hours (see ESI Section 3.3.1† for details). The reaction mixture was directly measured by ^{1}H NMR spectroscopy at 0, 24, 48, and 72 h time points (Fig. S19c, S20 and S21†), revealing a decrease in intensity of the coumarin peaks from the C_{10}-**Coumarin-bdcH$_2$** monomer over time, as well as the emergence of new aromatic signals from 6.2–7.8 ppm and new alkyl signals from 3.6–4.3 ppm. Cycloaddition

reactions between monomeric coumarin derivatives can afford up to four structural isomers – namely, *syn*-head-to-head, *syn*-head-to-tail, *anti*-head-to-head, and *anti*-head-to-tail – with the ratio of isomers determined by the structure of the coumarin derivative, concentration, and solvent conditions (Fig. S19a†).[50] To assign the emerging aromatic peaks to the formation of a mixture of coumarin dimer isomers, the final reaction mixture was further characterized by correlated spectroscopy (COSY) (Fig. S23 and S24†), enabling an assignment of the correlations between emerging proton signals, and therefore, differentiating the isomers from each other. Under these reaction conditions, three sets of correlated aromatic peaks were observed, each with splitting patterns and relative integrations consistent with the expected structures of the cycloaddition adducts. Meanwhile, the emerging alkyl signals can be attributed to the newly formed cyclobutane rings of the coumarin dimers, though the peaks are heavily overlapping, precluding differentiation of the signals corresponding to each isomer observed in the aromatic region. Note that this analysis does not allow us to assign each set of NMR signals to the absolute stereochemical configuration of a particular isomer. Such assignments would require the dimer isomers to be separated chromatographically, then crystallized for single-crystal X-ray diffraction analysis.[51] By comparing the relative integrations of dimer peaks to those of the residual C_{10}-**Coumarin-bdcH$_2$** monomer, a yield of 83% was calculated for the photodimerization reaction. To further confirm the formation of coumarin dimers, UV-Vis spectra of the reaction mixture were collected at each irradiation time point (Fig. S19b†), revealing a 72% decrease in the strong absorption peak at $\lambda = 320$ nm, which corresponds to a $\pi \rightarrow \pi^*$ transition of the coumarin monomer,[52] after UV exposure. By subtracting the absorbance contribution of the isophthalic acid subunit from the spectrum of C_{10}-**Coumarin-bdcH$_2$** and comparing the absorbance values before and after irradiation (see ESI Section 4.1† for detailed calculations), an 80% yield was calculated for the photodimerization reaction based on the UV-Vis data, which is in excellent agreement with the ^{1}H NMR results. Collectively, these findings demonstrate the photodimerization of the C_{10}-**Coumarin-bdcH$_2$** monomer, and highlight the possibility of achieving similar reactivity on the MOP surface.

Having established the photoreactivity of C_{10}-**Coumarin-bdcH$_2$** in solution, we investigated the dimerization of coumarin residues tethered to the C_{10}-**Coumarin-RhMOP** surface. A 5 mM solution of C_{10}-**Coumarin-RhMOP** in DMF-d$_7$ was irradiated (350 nm, 4 mW cm^{-2}) for 72 h, and ^{1}H NMR spectra were collected at 0, 24, 48, and 72 h time points to track the progress of the reaction (Fig. 3b and S25†). Sharp signals attributable to monomeric coumarin residues gradually decreased over time, while six new aromatic peaks and two new cyclobutane peaks appeared. COSY spectroscopy measurements revealed that the new aromatic peaks can be divided into two sets of three correlated protons (Fig. S26 and S27†), consistent with the formation of two coumarin dimer isomers (Fig. 3a), rather than the three observed upon irradiation of free C_{10}-**Coumarin-bdcH$_2$**. ^{13}C NMR spectra of the reaction mixture were also assigned through heteronuclear single quantum coherence (HSQC) and heteronuclear multiple bond correlation (HMBC)

experiments, and further demonstrate the emergence of two sets of correlated coumarin dimer signals (Fig. S28–S32†). UV-Vis spectroscopy measurements revealed a gradual loss of C_{10}-**Coumarin-RhMOP** absorption intensity at 320 nm upon exposure to 350 nm light, corresponding to a photodimerization yield of 68% at 72 h (Fig. 3c). Notably, DOSY NMR spectra of the reaction collected at 0 h ($D = 7.53 \times 10^{-11}$ m^2 s^{-1}) and 72 h ($D = 3.34 \times 10^{-11}$ m^2 s^{-1}) of UV exposure revealed a slight increase in the average hydrodynamic radius of the diffusing species from 3.6 nm to 8.2 nm (Fig. S3 and S33†), suggesting that intramolecular coumarin dimerization on the surface of a single cage is dominant at low concentration, but that increasing the reaction concentration might favor the formation of inter-cage crosslinks. We speculate that the preorganization of coumarin chains around the surface of the MOP favors the formation of head-to-head dimer isomers, particularly at low to moderate MOP concentrations, where intra-cage reactivity is dominant.

To investigate the direct photopolymerization of C_{10}-**Coumarin-RhMOPs** at elevated concentration, we prepared a 20 mM solution of C_{10}-**Coumarin-RhMOP** in DMF and irradiated the sample at 350 nm (10 mW cm^{-2}) for 12 h, at which point a thin, insoluble green film had formed at the surface facing the light source (Fig. S34†). After washing with DMF and methanol, the film was activated *via* supercritical CO$_2$ drying and imaged by scanning electron microscopy (SEM, Fig. 3d–f), revealing a dense cross-section with no visible macropores. Notably, the film was found to exhibit one smooth surface and one rough surface. We speculate that the smooth surface corresponds to the face of the film facing the light source, where a greater number of photons are absorbed by the MOP solution, leading to a greater density of crosslinks. To demonstrate the presence of coumarin dimers within the thin film, samples of pristine C_{10}-**Coumarin-RhMOP** and the photopolymerized film were characterized by IR spectroscopy (Fig. S35†). These measurements revealed that the carbonyl stretch at 1730 cm^{-1} broadens to higher wavenumber, and the C=C stretch at 1610 cm^{-1} decreases in intensity after irradiation, consistent with the conversion of coumarin's α,β-unsaturated carbonyl into a cyclobutane adduct. Collectively, these results demonstrate the efficient photodimerization of RhMOP-bound coumarin side chains, where a sufficiently high cage concentration enables the direct polymerization of dense thin films.

To investigate the relationship between the number of coumarin side chains attached to the MOP surface, as well as their bridging alkyl chain length, on their photodimerization efficiency, two additional cuboctahedral Coumarin-RhMOPs were prepared *via* solvothermal conditions analogous to those used for C_{10}-**Coumarin-RhMOP** (see ESI Section 2.2† for complete synthetic conditions). First, we synthesized the C_3-**Coumarin-RhMOP** (composed of $[Rh_2(C_3$-Coumarin-bdc)$_2]_{12}$), in which the alkyl chain bridging the isophthalic acid and coumarin residues was shortened to three carbons, and a methyl group was installed at the β-position relative to the lactone (Fig. S8†). Second, we reacted a 1 : 1 mixture of C_{10}-**Coumarin-bdcH$_2$** and 5-hydroxyisophthalic acid with dirhodium acetates to prepare 12 : 12 C_{10}-**Coumarin/OH-RhMOP** (Fig. S14†), which is a statistical mixture of cages with variable
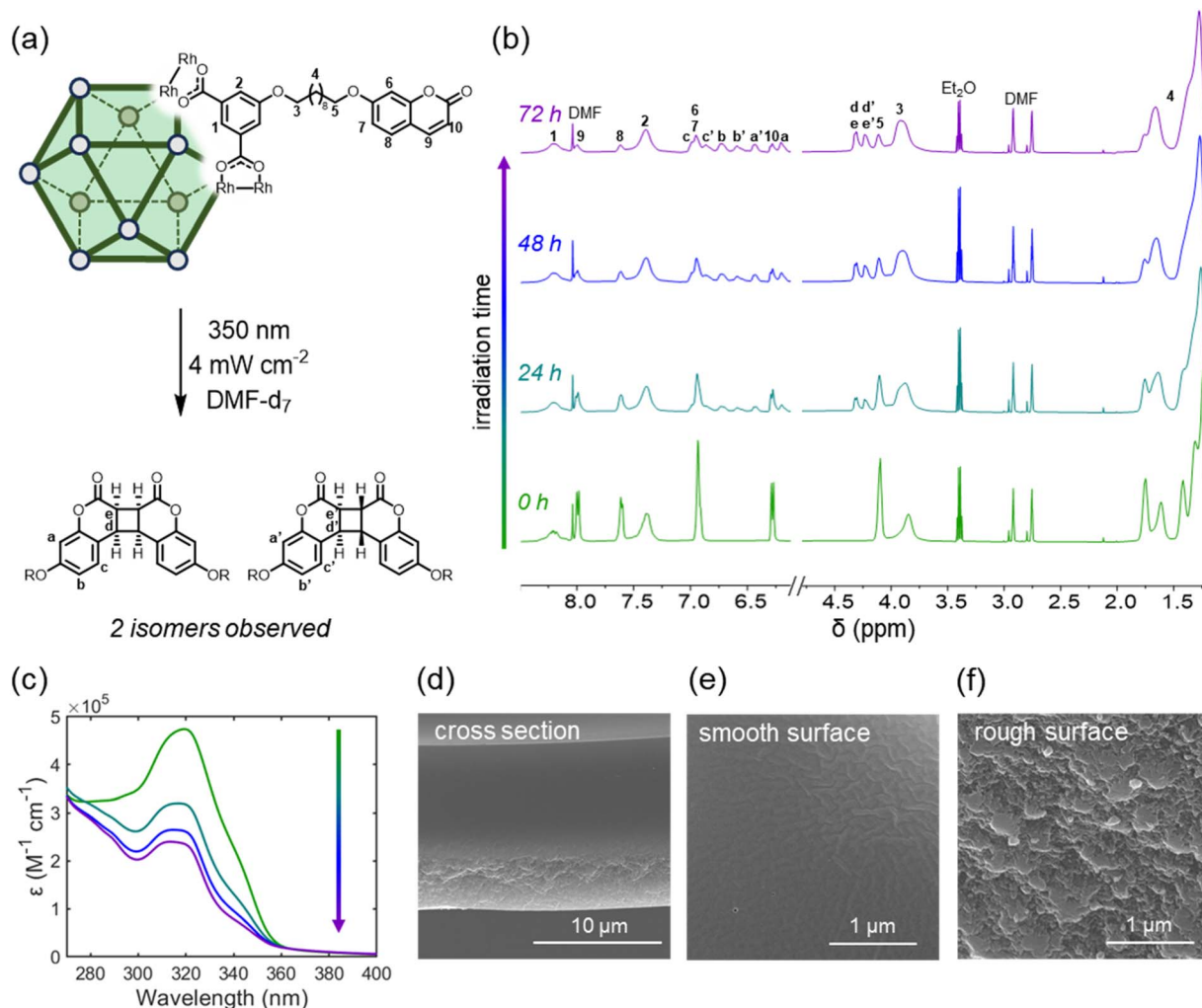
Fig. 3 (a) Irradiation of C_{10}-Coumarin-RhMOPs at 350 nm results in the dimerization of their side chains. (b) ^1H NMR spectra of a 5 mM DMF-d_7 solution of C_{10}-Coumarin-RhMOP after irradiation at 350 nm for 0 h (green), 24 h (teal), 48 h (blue), and 72 h (purple) reveal the emergence two correlated sets of aromatic and alkyl signals, suggesting the formation of two coumarin dimer isomers. Note that the absolute stereochemical configurations of the dimer isomers corresponding to each set of correlated peaks cannot be verified by this technique, and are therefore assigned arbitrarily. (c) UV-Vis spectra of the MOP solution at each irradiation time point reveal a decrease in the coumarin $\pi \rightarrow \pi^*$ peak at 320 nm, corroborating the formation of cyclobutane dimers. (d–f) SEM images of the (d) cross section, (e) smooth surface, and (f) rough surface of a photopolymerized C_{10}-Coumarin-RhMOP thin film produced via 350 nm irradiation of a 20 mM DMF solution of the cage.

coumarin loadings, centered at 12 coumarin side chains per MOP. DOSY data, mass spectra, and UV-Vis titration data for both samples supported the formation of the targeted cuboctahedra (Fig. S9–S12 and S15–S17†). DMF solutions of each cage at both 0.4 mM and 0.8 mM concentrations, where intra-MOP coumarin dimerization is dominant, were separately prepared and irradiated at 350 nm for 12 h (10 mW cm^{-2}). Based on the absorption intensity of the $\pi \rightarrow \pi^*$ band of the coumarin monomer (320 nm), which reflects the reaction yield, before and after irradiation, quantum yields (Φ_{dim}) and percent yields for the photodimerization event were calculated under each set of conditions (Fig. S37, see ESI Sections 4.1 and 4.2† for detailed calculations). Among the 0.8 mM solutions, C_{10}-Coumarin-RhMOP exhibited the highest quantum yield ($\Phi_{dim} = 0.0051$, 65% yield), followed by 12 : 12 C_{10}-Coumarin/OH-RhMOP ($\Phi_{dim} = 0.0021$, 54% yield), and then C_3-Coumarin-RhMOP ($\Phi_{dim} =$

0.0013, 17% yield). We speculate that the higher quantum yield observed for C_{10}-Coumarin-RhMOP relative to the other cages is attributed to the greater density and flexibility of the coumarin side chains. Higher coumarin density places the molecules on the surface of the cage in closer proximity, while longer bridging alkyl chain length provides MOP-bound coumarins with greater flexibility to adopt the intermolecular arrangements required for cycloaddition to occur.[49] When the reaction concentration was decreased to 0.4 mM, C_3-Coumarin-RhMOP maintained a nearly equivalent quantum yield of $\Phi_{dim} = 0.0015$ (39% yield), indicating that lowering the MOP concentration does not impact the efficiency of photodimerization. This concentration independence is likely due to the preorganization of coumarin side chains at high local densities on the MOP surface. To our initial surprise, when the 0.4 mM solutions of C_{10}-Coumarin-RhMOP and 12 : 12 C_{10}-Coumarin/OH-RhMOP were irradiated

at 350 nm, quantum yields of Φ_{dim} = 0.0030 (76% yield) and Φ_{dim} = 0.0012 (60% yield), respectively, were obtained, representing substantial decreases compared to the 0.8 mM solutions of the same cages. To investigate this discrepancy, we prepared and irradiated a 0.6 mM DMF solution of C_{10}-Coumarin-RhMOP, which provided a quantum yield (Φ_{dim} = 0.0041) similar to the 0.8 mM solution, as well as a reaction yield (74%) equivalent to the 0.4 mM solution (Fig. S38†). Based on the equivalent reaction yields obtained for 0.4 and 0.6 mM solutions under identical irradiation conditions, we speculate that the reaction proceeds efficiently until ∼75% of the coumarin side chains have dimerized (or ∼60% of the side chains for the 12 : 12 C_{10}-Coumarin/OH-RhMOP), at which point the surface density of unreacted coumarin is sufficiently low that intra-MOP dimerization no longer occurs. At low concentrations (<5 mM), inter-MOP crosslinking is sterically precluded, meaning that subsequent excitation is unproductive, leading to a decrease in the calculated quantum yields for the 0.4 mM samples. To further clarify the influence of MOP surface preorganization on quantum yields for coumarin dimerization, we performed identical irradiation control experiments with DMF solutions of C_{10}-Coumarin-bdcH$_2$ at 10 mM and 20 mM concentrations (Fig. S37d†), which contain the same absolute coumarin concentration as the 0.4 mM and 0.8 mM C_{10}-Coumarin-RhMOP solutions, respectively. For 10 mM and 20 mM C_{10}-Coumarin-bdcH$_2$ solutions, quantum yields of Φ_{dim} = 0.0009 (23% yield) and Φ_{dim} = 0.0017 (22% yield), respectively, were obtained, both of which are significantly lower than those measured for analogous C_{10}-Coumarin-RhMOP solutions. This result is consistent with our understanding that a high local density of coumarin moieties increases the probability of a photoexcited molecule reacting productively with an adjacent ground-state molecule. This conclusion is further supported by the increase in dimerization quantum yield observed when the C_{10}-Coumarin-bdcH$_2$ concentration was increased from 10 mM to 20 mM. Collectively, these results establish the effects of bridging alkyl chain length and coumarin density on Coumarin-RhMOP photodimerization efficiency, and highlight the high-yielding C_{10}-Coumarin-RhMOP as an ideal building block for constructing porous soft materials through dual coordination/covalent polymerization.

Coordination and covalent polymerization of Coumarin-RhMOP gels

Cuboctahedral RhMOPs possess exohedral open metal sites, which enable their coordination-driven polymerization in the presence of ditopic crosslinkers (Fig. 4a), affording hierarchically porous colloidal gels.[14,28,29,31,33] Given that a high local concentration of Coumarin-RhMOPs is necessary to achieve their efficient photopolymerization, we envisioned that preorganizing the cages into a colloidal gel through an analogous coordination-based polymerization protocol, followed by photocrosslinking the preformed network covalently, should lead to doubly crosslinked porous networks with superior stability. We identified 1,4-bis(imidazol-1-ylmethyl)benzene, also known as bix (Fig. 4a, blue), as an ideal ditopic ligand for constructing photopolymerizable Coumarin-RhMOP gels, since bix is sufficiently rigid to support MOP gelation and includes fewer UV-absorbing aromatic rings compared to other common coordination crosslinkers.[29,53,54]

Towards photopolymerizable MOP gels, a 0.4 mM DMF solution of C_{10}-Coumarin-RhMOP was mixed rapidly with 12 equivalents of bix, affording a purple solution of (C_{10}-Coumarin-RhMOP)(bix)$_{12}$, in which each bix molecule coordinated to a single open metal site in a monodentate fashion. The reaction mixture was then heated at 80 °C for 72 hours, at which point the solution had solidified into a transparent, purple gel (hereafter termed bix gel). The gel was first washed with fresh DMF to remove unbound bix molecules, then exchanged with methanol and activated by supercritical CO$_2$ drying, affording the corresponding bix aerogel. SEM images of the aerogel revealed a hierarchically porous, fused colloidal morphology (Fig. 4b), consistent with prior research on the coordination-driven assembly of RhMOPs.[29,33] To estimate the degree of coordination crosslinking within the aerogel, the dirhodium paddlewheels were decomposed via heating in a DMSO-d$_6$/D$_2$O/DCl mixture at 100 °C (see ESI Section 3.1.2† for detailed protocol), affording a mixture of bix and C_{10}-Coumarin-bdcH$_2$, which was then characterized via ^{1}H NMR spectroscopy. Relative integrations of bix and C_{10}-Coumarin-bdcH$_2$ signals indicated an aerogel composition of (C_{10}-Coumarin-RhMOP)(bix)$_{5.6}$ (Fig. S40†). These findings demonstrate that rigid, ditopic imidazoles can be employed to organize Coumarin-RhMOPs into hierarchically porous colloidal networks, which could serve as templates for the photopolymerization of robust, covalent MOP gels.

To photocrosslink bix gel, the as-synthesized gel was first submerged in a shallow pool of DMF to prevent solvent evaporation, then irradiated at 350 nm (4 mW cm^{-2}, 5 h), after which the gel became slightly redder in color (Fig. 4a). This color change can be attributed to a minor increase in absorption of the coumarin side chains at 400 nm upon dimerization (Fig. S19b†), providing a first indication that the photopolymerization was successful. To confirm the formation of cyclobutane crosslinks within the colloidal network, samples of MOP gel before (bix gel) and after (coumarin/bix gel) irradiation were activated by supercritical CO$_2$ drying, and the corresponding aerogels were characterized by IR spectroscopy and ^{13}C cross-polarization magic angle spinning (CP/MAS) NMR spectroscopy. IR spectra of bix aerogel (Fig. S44,† purple) and coumarin/bix aerogel (Fig. S44,† red) revealed that the C=O stretch at 1730 cm^{-1} broadens towards higher wavenumber upon exposure to UV light, consistent with the loss of α,β-unsaturation at the coumarin carbonyl that accompanies cyclobutane crosslink formation. Furthermore, the intensity of the C=C stretch at 1610 cm^{-1} decreased after irradiation, consistent with the formation of cycloaddition adducts. Likewise, ^{13}C CP/MAS NMR spectra of both aerogels (Fig. 4c) reveal the emergence of a new signal at 40 ppm after irradiation, which corresponds to the cyclobutane carbons of the coumarin dimer. This peak position is in excellent agreement with the cyclobutane peaks of intramolecular MOP-bound coumarin dimers observed in ^{13}C NMR spectra of UV-irradiated solutions of C_{10}-
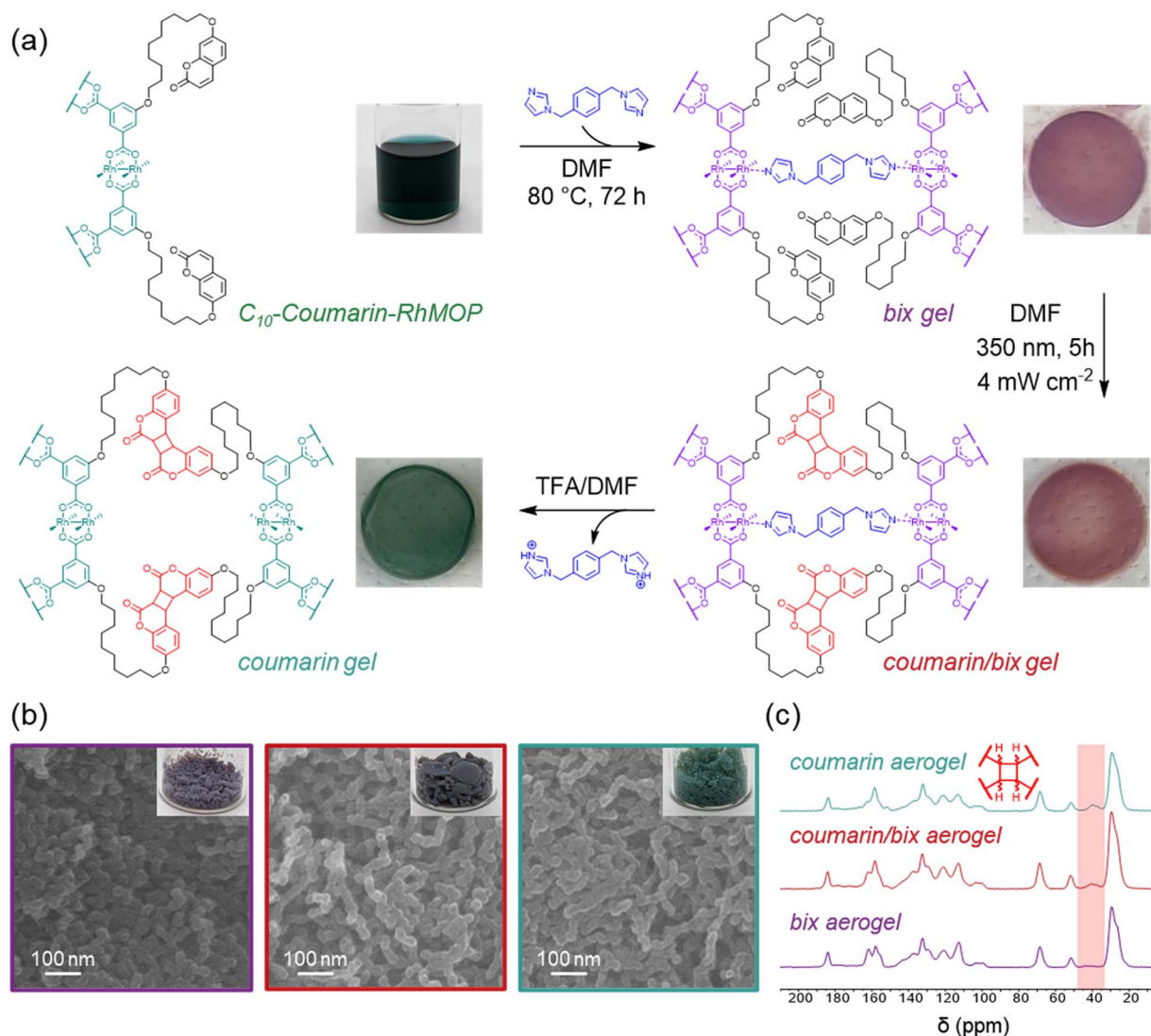
Fig. 4 (a) Overview of bix-mediated gelation and photopolymerization protocols for **C$_{10}$-Coumarin-RhMOPs**. Photos of each solution and gel formed throughout the process are provided beside each chemical structure. (b) SEM images of **bix** (purple), **coumarin/bix** (red), and **coumarin** (teal) aerogels after supercritical CO$_2$ activation reveal that the fused colloidal morphology characteristic of coordination-linked MOP gels is preserved upon photoirradiation and subsequent bix dissociation. (c) ^{13}C CP/MAS NMR spectra of **bix**, **coumarin/bix**, and **coumarin** aerogels reveal the emergence of a characteristic cyclobutane signal at 40 ppm after photoirradiation, which is preserved upon bix dissociation.

Coumarin-RhMOP (Fig. S28†). Taken together, these data demonstrate that Coumarin-RhMOP/bix gels support [2 + 2] cycloaddition reactions between MOP-bound coumarin side chains.

To obtain MOP gels bearing open rhodium sites on the cage surfaces, we sought to dissociate bix from the irradiated **coumarin/bix gels** by protonating their imidazole linkers, according to literature precedent.[31] The addition of a 10 : 1 v/v DMF/trifluoroacetic acid (TFA) mixture to a sample of **coumarin/bix gel** resulted in a rapid color change from purple to green (Fig. 4a and S39†), providing a first indication of coordination crosslinker dissociation. A portion of the gel (∼40 wt%) dissolved upon acid addition to afford a green/blue solution, likely due to limited UV light penetration into the core of the gel, but the majority of the gel remained intact. This remaining

green gel (hereafter termed **coumarin gel**) was washed with DMF and methanol, then activated by supercritical CO$_2$ drying, affording the corresponding **coumarin aerogel**, where the network is held together entirely through covalent cyclobutane crosslinks. To confirm the molecular compositions of **coumarin/bix aerogel** and **coumarin aerogel**, both samples were decomposed to their molecular constituents in DMSO-d$_6$/D$_2$O/DCl mixtures, then characterized by ^{1}H NMR spectroscopy (Fig. S40†). The irradiated **coumarin/bix aerogel** was found to exhibit a composition of (**C$_{10}$-Coumarin-RhMOP**)(bix)$_{5.6}$, in perfect agreement with the pristine bix aerogel. Note that these decomposition conditions also cleave the cyclobutane cross-links of the **C$_{10}$-Coumarin-bdcH$_2$** dimers (Fig. S42†), preventing their direct observation in the NMR spectrum. To our surprise, **coumarin aerogel** was found to be composed of (**C$_{10}$-Coumarin-**

RhMOP)(bix)$_{2.4}$ after treatment with DMF/TFA for 12 h, indicating that the wash protocol only removed 60% of the bix molecules. In an attempt to fully remove bix from the network, four additional **coumarin aerogel** samples were prepared using harsher imidazole dissociation conditions, decomposed, and characterized by ^{1}H NMR spectroscopy (Fig. S43, details in ESI Section 2.3.8†). In all cases, the corresponding aerogels were found to contain 1–2 molecules of bix per cage. Given that the gel changes color from purple to green upon acid exposure, and residual unreacted MOP dissolves, we speculate that the remaining bix molecules are not coordinated to the cages, but are otherwise trapped within the porous network or interacting with coumarin moieties through intermolecular forces.

SEM images of **coumarin/bix aerogel** and **coumarin aerogel** both reveal fused colloidal morphologies identical to that observed for the pristine **bix gel** (Fig. 4b), indicating that the photopolymerization and bix dissociation processes do not compromise the mesoscale colloidal network structures. To confirm the presence of cyclobutane crosslinks within **coumarin aerogel**, the sample was analyzed by both IR spectroscopy and ^{13}C CP/MAS NMR spectroscopy. Like the irradiated **coumarin/bix aerogel**, the **coumarin aerogel** IR spectrum exhibited a broadened C=O stretch at 1730 cm^{-1} and a weak C=C stretch at 1610 cm^{-1} compared to the pristine **bix gel**, indicating the presence of coumarin dimers in the network (Fig. S44†). Moreover, the ^{13}C CP/MAS NMR spectrum of **coumarin aerogel** contained a strong cyclobutane carbon signal at 40 ppm, demonstrating that the cyclobutane crosslinks are preserved during acid treatment (Fig. 4c).

To further validate the role of coumarin side chains in the photopolymerization of Coumarin-RhMOP/**bix gels**, we prepared an equivalent bix-linked gel using an unfunctionalized RhMOP without coumarin side chains (HRhMOP, composed of [Rh$_2$(H-bdc)$_2$]$_{12}$),[28,55] and irradiated the sample under identical conditions (350 nm 4 mW cm^{-2}, 5 h). After irradiation, the HRhMOP/bix gel was treated with DMF/TFA, resulting in its immediate and complete dissolution to a blue/green solution (Fig. S45†). This result demonstrates that RhMOP/bix gels are incapable of reacting under UV-irradiation in the absence of coumarin side chains, and confirms our understanding of the photopolymerization mechanism.

To demonstrate that **coumarin gel** contains accessible exohedral open metal sites, we added a prototypical N-donor ligand, pyridine, to a sample of **coumarin gel**, which resulted in its immediate color change from green to purple/red, indicative of dirhodium paddlewheel coordination. Notably, subsequent treatment with DMF/TFA resulted in the reversal of the color from purple to green, suggesting that **coumarin gels** can be reversibly functionalized through the coordination and dissociation of N-donor ligands (Fig. S46†). Taken together, these results demonstrate that pristine **bix gel** can serve as a template for the photopolymerization of chemically stable, covalently crosslinked Coumarin-RhMOP gels bearing accessible open metal sites.

Properties of Coumarin-RhMOP gels

Coordination-driven gelation of cuboctahedral RhMOPs typically requires the use of short ditopic ligands as crosslinkers, since short linkers are unable to complex two dirhodium paddlewheels on the same cage. One disadvantage of this approach is that short linkers typically produce brittle gels, which are prone to fracture under low mechanical strain.[21,24,29,33] Indeed, we observed that pristine **bix gels** are easily fractured when transferring between reaction vessels, and do not deform substantially when swirled in DMF (Video S1†). **Coumarin/bix gels** were also found to hold their shape when agitated in DMF (Video S2†), but were more resistant to fracture, and could be folded and unfolded without cracking. In contrast, **coumarin gel** was observed to be highly deformable, and readily changed its shape when swirled in DMF (Video S3†). This behavior is unusual for MOP gels and prompted us to evaluate their mechanical properties quantitatively through rheological measurements.

In particular, we chose to pursue shear rheology, as this configuration can be applied to thin layers of MOP gel, where UV light can penetrate through the sample during photopolymerization. First, we performed angular frequency sweep tests, in which the oscillatory frequency of the probe was varied from $\omega = 0.1$–10 rad s^{-1} at a fixed strain amplitude of $\gamma = 1\%$, to quantify the storage (G') and loss (G'') moduli of **bix gel**, **coumarin/bix gel**, and **coumarin gel** in DMF (Fig. 5a). For each sample, G' was observed to be approximately ten times higher than G'' and frequency-independent, as is characteristic for crosslinked polymer gels. Notably, the average G' value of **coumarin gel** (12 Pa) was far lower than that of **bix gel** (64 Pa) and **coumarin/bix gel** (116 Pa), confirming our initial observation that **coumarin gel** is more deformable than its bix-linked counterparts. We attribute this deformability to the flexible decyl chains connecting each photopolymerizable coumarin unit to the backbone of the **C$_{10}$-Coumarin-RhMOP**, which provides more conformational freedom compared to the relatively rigid aromatic backbone of bix. Since **coumarin gel** includes newly opened rhodium sites on the surface of each cage, we envisioned that it might be possible to stiffen the network through the readdition of ditopic imidazole linkers. To test this hypothesis, 12 stoichiometric equivalents of bix were added to a sample of **coumarin gel**, resulting in the saturation of each cage with monodentate bix, as well as a visible color change from green to purple. The gel was then heated for 6 h to induce the partial dissociation of monodentate bix from the surface of each MOP, promoting the reformation of coordination crosslinks between cages. The resulting doubly crosslinked gel (hereafter called **bix re-added gel**) exhibited an average G' value of 99 Pa, representing a near-complete recovery of the storage modulus of pristine **coumarin/bix gel** (Fig. 5a). To investigate the mechanical strength of each gel, we further performed strain amplitude sweep tests, in which the oscillatory frequency was fixed at $\omega = 1$ rad s^{-1} while the strain amplitude was gradually increased from $\gamma = 0.1$–400% (Fig. S47†). In all measurements, we used the G'' peak as a practical indicator of the onset of fracture to compare the
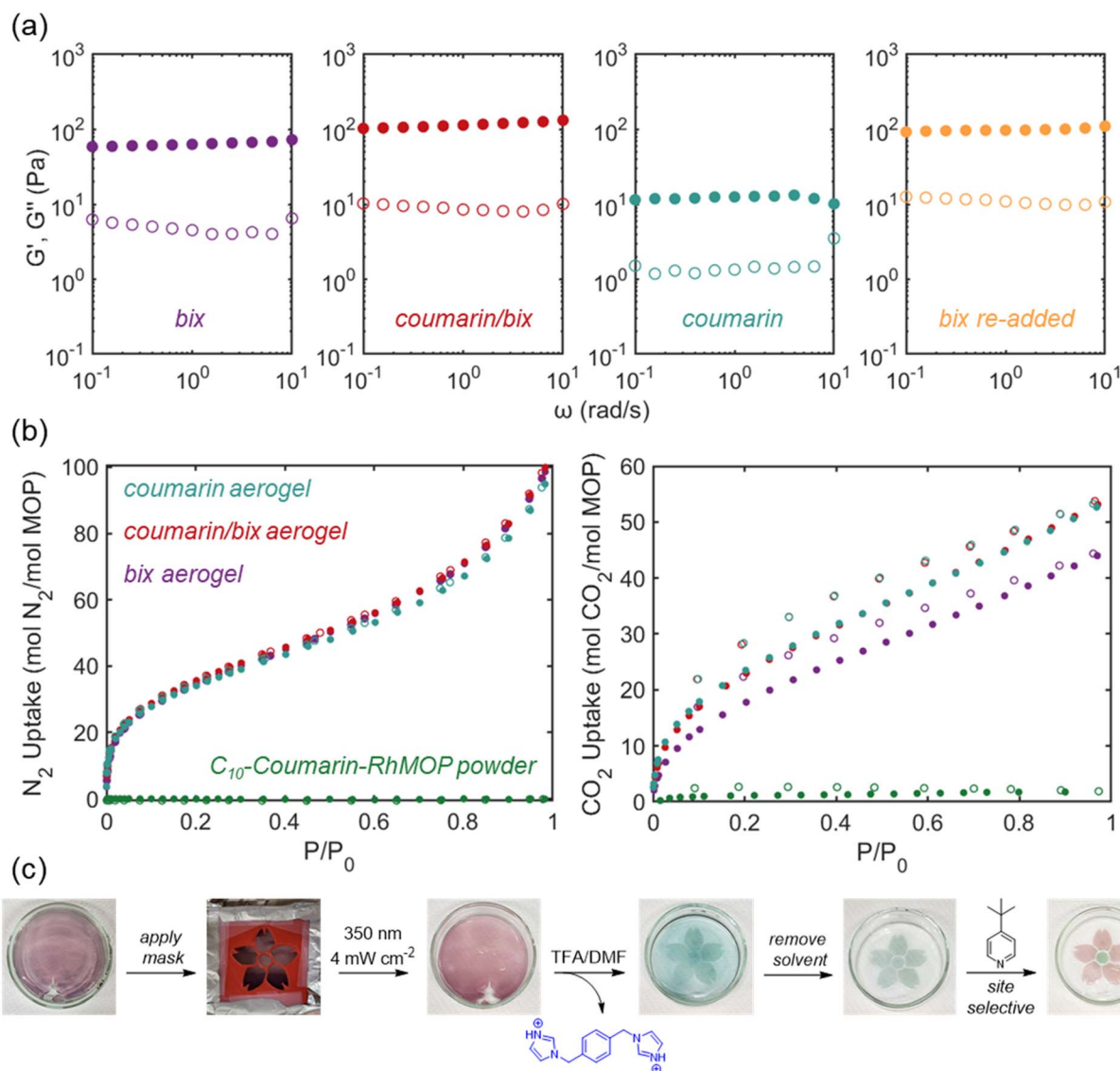
Fig. 5 (a) Angular frequency sweep measurements of **bix** (purple), **coumarin/bix** (red), **coumarin** (teal), and **bix re-added** (yellow) gels in DMF reveal that their storage moduli (G', filled circles) are each an order of magnitude larger than their loss moduli (G'', open circles) and frequency independent, as expected for crosslinked polymer gels. (b) N_2 (left) and CO_2 (right) adsorption (filled circles) and desorption (open circles) isotherms for **bix**, **coumarin/bix**, and **coumarin** aerogels after supercritical CO_2 activation reveal their equivalent hierarchical porosity. On the contrary, vacuum-activated C_{10}-**Coumarin-RhMOP** powder (green) shows negligible uptake of both N_2 and CO_2, suggesting that the intrinsic pores are blocked by the dense canopy of coumarin side chains. (c) Site-selective UV-irradiation of **bix** gel, followed by bix dissociation, enables the preparation of photopatterned covalent **coumarin** gel, which can be subsequently functionalized with N-donor ligands.

mechanical strength of the gels. Pristine **bix gel** began to fracture at a relatively low strain amplitude of $\gamma = 25\%$, whereas photoirradiated **coumarin/bix** gel maintained its integrity up to a higher strain amplitude of $\gamma = 63\%$. We speculate that the greater strength of **coumarin/bix** gel can be attributed to the flexible coumarin crosslinks, which can hold the gel together even if the mechanical stress induces the partial dissociation of the rigid coordination crosslinkers. Covalent **coumarin gel** began to fracture at an even higher strain of $\gamma = 101\%$. One possible explanation is that the dissociation of bix from the network allows the dimerized coumarin side chains to relax into a less entangled and more conformationally flexible

configuration, providing a more strain-tolerant gel structure. We also note that **coumarin/bix gels** contain some cages that do not photopolymerize upon UV exposure due to limited light penetration, which might contribute to their onset of fracture at lower strain amplitudes. Consistent with the above results, **bix re-added gel** also provided a high fracture onset strain ($\gamma = 159\%$). Taken together, these experiments demonstrate that the addition and dissociation of ditopic imidazole crosslinkers can reversibly regulate the stiffness and strength of photopolymerized Coumarin-RhMOP gels, providing unprecedented control of their mechanical properties through orthogonal crosslink chemistries.

Covalent Coumarin-RhMOP gels retain their hierarchical porosity after coordination crosslinker dissociation and supercritical CO_2 activation, as verified by gas sorption experiments. To investigate the porosity of the **bix**, **coumarin/bix**, and **coumarin aerogels**, as well as pristine **C_{10}-Coumarin-RhMOP** powder, each was characterized through N_2 and CO_2 sorption measurements (Fig. 5b). **C_{10}-Coumarin-RhMOP** powder was found to be nonporous to both N_2 and CO_2, which we attribute to the dense canopy of alkyl-tethered coumarin side chains attached to the MOP surface. Long, flexible side chains can block the narrow pore windows of the MOP and prevent gas molecules from diffusing into the cage cavity. Such behavior was previously observed for a structurally analogous cuboctahedral RhMOP functionalized with dodecyl chains.[29] In contrast, all three aerogel samples exhibited nearly identical N_2 sorption isotherms, with BET surface areas of 189, 193, and 193 $m^2 g^{-1}$ calculated for **bix**, **coumarin/bix**, and **coumarin aerogels**, respectively, *via* BETSI analysis (Fig. S66–68†).[56] These values are similar to those observed for other RhMOPs functionalized with extended side chains, and demonstrate that the porosity of the MOP network is fully maintained throughout the photopolymerization and bix dissociation processes. CO_2 adsorption isotherms for all three aerogels also showed similar behavior, with slightly higher gas uptake observed for **coumarin/bix** and **coumarin aerogels** relative to the pristine **bix gel**. Collectively, these measurements demonstrate that coumarin-mediated photopolymerization and coordination crosslinker dissociation preserves the hierarchical porosity and guest uptake capabilities characteristic of imidazole-linked RhMOP gels.

One major advantage of light-mediated chemical transformations is that they can be initiated with spatiotemporal control. In the case of porous materials, photopatterning could be leveraged to construct structurally-defined nanoporous chemical reactors for use in catalysis,[57] sensors,[58] or shaped scaffolds for tissue engineering.[16] To highlight this possibility for our materials, we sought to photopattern covalent **coumarin gels** through the site-selective irradiation of preorganized **bix gels** with UV light. As a proof-of-concept, we prepared a sample of **bix gel** in a 6 cm Petri dish, covered the surface of the gel with a cherry blossom-shaped photomask, and irradiated the exposed surface at 350 nm (4 mW cm^{-2}, 5 h). Subsequent addition of a TFA/DMF solution to remove bix resulted in the dissolution of the masked portions of the gel, while the irradiated, cherry blossom-shaped center of the gel remained intact and changed color from purple to green. Removal of the unreacted MOP solution *via* pipette afforded the isolated, patterned **coumarin gel**, in which the flower core and petals were well-resolved (Fig. 5c).

Another unique feature of our photopatterned **coumarin gels** is that each component MOP contains open rhodium coordination sites on its surface, which can be leveraged for the reversible, postsynthetic modification of the gel backbone through the coordination and dissociation of N-donor ligands. To demonstrate the site-selective functionalization of **coumarin gel**, we carefully deposited 4-*t*-butylpyridine onto the petals of the cherry blossom, resulting in their immediate color change from green to purple, corresponding to the coordination of the ligands to the cages' exohedral open metal sites. At the same time, the core of the gel, to which 4-*t*-butylpyridine was not added, remained green and unfunctionalized (Fig. 5c). These results highlight the opportunity to construct porous networks with high structural and functional complexity through the preorganization and photopolymerization of a single, discrete metal–organic polyhedron.

Conclusions

In conclusion, we demonstrated the synthesis of three new RhMOPs covalently grafted with photodimerizable coumarin side chains (**C_{10}-Coumarin-RhMOP**, **C_3-Coumarin-RhMOP**, and 12 : 12 **C_{10}-Coumarin/OH-RhMOP**), as verified by NMR spectroscopy, UV-Vis spectroscopy, and mass spectrometry experiments. Irradiation of low-concentration RhMOP solutions at 350 nm triggered the intramolecular dimerization of their coumarin side chains, with **C_{10}-Coumarin-RhMOP** exhibiting the highest dimerization quantum yield due to the high density and conformational flexibility of the coumarin chains. Irradiation of high-concentration **C_{10}-Coumarin-RhMOP** solutions enabled their direct polymerization into dense thin films connected entirely through cyclobutane crosslinks. In contrast, coordination-driven polymerization of **C_{10}-Coumarin-RhMOP** into a colloidal gel, followed by site-selectively irradiation, afforded dual coordination/covalent RhMOP gels, which exhibited equivalent porosity and greater mechanical strength compared to their solely coordination-linked counterparts. Dissociation of coordination crosslinkers from the doubly crosslinked networks afforded solely covalent Coumarin-RhMOP gels, which are among the most readily deformable and chemically robust MOP gels reported to date, with structures and mechanical properties that can be reversibly tuned through the coordination of their open rhodium sites with Lewis bases. These findings establish coumarin-mediated photopolymerization as a powerful method for assembling mechanically tunable, structurally diverse porous materials from solution-processable molecular pores, and open up new opportunities to incorporate complex functionality into this emergent class of amorphous porous networks.

Data availability

The data supporting this article have been included as part of the ESI.†

Author contributions

D. W. B. and S. F. conceived and designed the project. D. W. B. synthesized all materials, and contributed to the collection and interpretation of all structural characterization data. D. W. B., M. Y., M. K., and K. U. performed the rheological measurements. Z. W. assisted with the collection of the gas sorption isotherms. K. S. provided guidance related to the development of solution-state and solid-state photopolymerization protocols for Coumarin-RhMOP materials. D. W. B. and S. F. drafted the manuscript, and all authors contributed to its revision.

Conflicts of interest

The authors declare no competing financial interests.

Acknowledgements

Notes and references

1 J. R. Werber, C. O. Osuji and M. Elimelech, Materials for next-generation desalination and water purification membranes, *Nat. Rev. Mater.*, 2016, **1**, 16018.

2 T. Kim, J.-H. Kim, T. E. Kang, C. Lee, H. Kang, M. Shin, C. Wang, B. Ma, U. Jeong, T.-S. Kim and B. J. Kim, Flexible, highly efficient all-polymer solar cells, *Nat. Commun.*, 2015, **6**, 8547.

3 A. J. T. Teo, A. Mishra, I. Park, Y.-J. Kim, W.-T. Park and Y.-J. Yoon, Polymeric Biomaterials for Medical Implants and Devices, *ACS Biomater. Sci. Eng.*, 2016, **2**, 454–472.

4 S. Wang, H. Li, H. Huang, X. Cao, X. Chen and D. Cao, Porous organic polymers as a platform for sensing applications, *Chem. Soc. Rev.*, 2022, **51**, 2031–2080.

5 M. Haktaniyan and M. Bradley, Polymers showing intrinsic antimicrobial activity, *Chem. Soc. Rev.*, 2022, **51**, 8584–8611.

6 M. B. Wandel, C. A. Bell, J. Yu, M. C. Arno, N. Z. Dreger, Y.-H. Hsu, A. Pitto-Barry, J. C. Worch, A. P. Dove and M. L. Becker, Concomitant control of mechanical properties and degradation in resorbable elastomer-like materials using stereochemistry and stoichiometry for soft tissue engineering, *Nat. Commun.*, 2021, **12**, 446.

7 R. H. Alasfar, M. Koç, V. Kochkodan, S. Ahzi and N. Barth, Optimization of the elastic modulus for polymeric nanocomposite membranes, *J. Appl. Polym. Sci.*, 2024, **141**, e54883.

8 J. P. Gong, Why are double network hydrogels so tough?, *Soft Matter*, 2010, **6**, 2583–2590.

9 F. J. Maksoud, M. F. Velázquez de la Paz, A. J. Hann, J. Thanarak, G. C. Reilly, F. Claeyssens, N. H. Green and Y. S. Zhang, Porous biomaterials for tissue engineering: a review, *J. Mater. Chem. B*, 2022, **10**, 8111–8165.

10 D. W. Burke, Z. Jiang, A. G. Livingston and W. R. Dichtel, 2D Covalent Organic Framework Membranes for Liquid-Phase Molecular Separations: State of the Field, Common Pitfalls, and Future Opportunities, *Adv. Mater.*, 2024, **36**, 2300525.

11 A. J. Gosselin, C. A. Rowland and E. D. Bloch, Permanently Microporous Metal–Organic Polyhedra, *Chem. Rev.*, 2020, **120**, 8987–9014.

12 T. Tateishi, M. Yoshimura, S. Tokuda, F. Matsuda, D. Fujita and S. Furukawa, Coordination/metal–organic cages inside out, *Coord. Chem. Rev.*, 2022, **467**, 214612.

13 A. Khobotov-Bakishev, L. Hernández-López, C. von Baeckmann, J. Albalad, A. Carné-Sánchez and D. Maspoch, Metal–Organic Polyhedra as Building Blocks for Porous Extended Networks, *Adv. Sci.*, 2022, **9**, 2104753.

14 Z. Wang and S. Furukawa, Pore-Networked Soft Materials Based on Metal–Organic Polyhedra, *Acc. Chem. Res.*, 2024, **57**, 327–337.

15 A. Giri, A. Sahoo, T. K. Dutta and A. Patra, Cavitand and Molecular Cage-Based Porous Organic Polymers, *ACS Omega*, 2020, **5**, 28413–28424.

16 E. Nicol, Photopolymerized Porous Hydrogels, *Biomacromolecules*, 2021, **22**, 1325–1345.

17 S. M. Mantooth, B. G. Munoz-Robles and M. J. Webber, Dynamic Hydrogels from Host–Guest Supramolecular Interactions, *Macromol. Biosci.*, 2019, **19**, 1800281.

18 M. Galizia, W. S. Chi, Z. P. Smith, T. C. Merkel, R. W. Baker and B. D. Freeman, 50th Anniversary Perspective: Polymers and Mixed Matrix Membranes for Gas and Vapor Separation: A Review and Prospective Opportunities, *Macromolecules*, 2017, **50**, 7809–7843.

19 X. Li, W. Lin, V. Sharma, R. Gorecki, M. Ghosh, B. A. Moosa, S. Aristizabal, S. Hong, N. M. Khashab and S. P. Nunes, Polycage membranes for precise molecular separation and catalysis, *Nat. Commun.*, 2023, **14**, 3112.

20 X. Guo, S. Xu, Y. Sun, Z. Qiao, H. Huang and C. Zhong, Metal-organic polyhedron membranes for molecular separation, *J. Membr. Sci.*, 2021, **632**, 119354.

21 A. Khobotov-Bakishev, P. Samanta, K. Roztocki, J. Albalad, S. Royuela, S. Furukawa, F. Zamora, A. Carné-Sánchez and D. Maspoch, Post-Synthetic Modification of Aerogels Made of Covalent Cross-linked Metal-Organic Polyhedra, *Adv. Funct. Mater.*, 2024, **34**, 2312166.

22 J. Liu, W. Duan, J. Song, X. Guo, Z. Wang, X. Shi, J. Liang, J. Wang, P. Cheng, Y. Chen, M. J. Zaworotko and Z. Zhang, Self-Healing Hyper-Cross-Linked Metal–Organic Polyhedra (HCMOPs) Membranes with Antimicrobial Activity and Highly Selective Separation Properties, *J. Am. Chem. Soc.*, 2019, **141**, 12064–12070.

23 D. Nam, J. Huh, J. Lee, J. H. Kwak, H. Y. Jeong, K. Choi and W. Choe, Cross-linking Zr-based metal–organic polyhedra via postsynthetic polymerization, *Chem. Sci.*, 2017, **8**, 7765–7771.

24 M. L. Schneider, J. A. Campbell, A. D. Slattery and W. M. Bloch, Polymer networks of imine-crosslinked metal–organic cages: tuneable viscoelasticity and iodine adsorption, *Chem. Commun.*, 2022, **58**, 12122–12125.

25 M. Tonigold, J. Hitzbleck, S. Bahnmüller, G. Langstein and D. Volkmer, Copper(II) Nanoballs as monomers for polyurethane coatings: synthesis, urethane derivatization and kinetic stability, *Dalton Trans.*, 2009, 1363–1371.

26 X.-Y. Xie, F. Wu, X. Liu, W.-Q. Tao, Y. Jiang, X.-Q. Liu and L.-B. Sun, Photopolymerization of metal–organic polyhedra: an efficient approach to improve the hydrostability, dispersity, and processability, *Chem. Commun.*, 2019, **55**, 6177–6180.

27 J. Zhao, L. Cheng, K. Liu, Z. Zhang, W. Yu and X. Yan, Metal–organic polyhedra crosslinked supramolecular polymeric elastomers, *Chem. Commun.*, 2020, **56**, 8031–8034.

28 A. Carné-Sánchez, G. A. Craig, P. Larpent, V. Guillerm, K. Urayama, D. Maspoch and S. Furukawa, A Coordinative Solubilizer Method to Fabricate Soft Porous Materials from Insoluble Metal–Organic Polyhedra, *Angew. Chem., Int. Ed.*, 2019, **58**, 6347–6350.

29 A. Carné-Sánchez, G. A. Craig, P. Larpent, T. Hirose, M. Higuchi, S. Kitagawa, K. Matsuda, K. Urayama and S. Furukawa, Self-assembly of metal–organic polyhedra into supramolecular polymers with intrinsic microporosity, *Nat. Commun.*, 2018, **9**, 2506.

30 J. A. Foster, R. M. Parker, A. M. Belenguer, N. Kishi, S. Sutton, C. Abell and J. R. Nitschke, Differentially Addressable Cavities within Metal–Organic Cage-Cross-Linked Polymeric Hydrogels, *J. Am. Chem. Soc.*, 2015, **137**, 9722–9729.

31 A. Legrand, L.-H. Liu, P. Royla, T. Aoyama, G. A. Craig, A. Carné-Sánchez, K. Urayama, J. J. Weigand, C.-H. Lin and S. Furukawa, Spatiotemporal Control of Supramolecular Polymerization and Gelation of Metal–Organic Polyhedra, *J. Am. Chem. Soc.*, 2021, **143**, 3562–3570.

32 E. Sánchez-González, M. Y. Tsang, J. Troyano, G. A. Craig and S. Furukawa, Assembling metal–organic cages as porous materials, *Chem. Soc. Rev.*, 2022, **51**, 4876–4889.

33 Z. Wang, C. Villa Santos, A. Legrand, F. Haase, Y. Hara, K. Kanamori, T. Aoyama, K. Urayama, C. M. Doherty, G. J. Smales, B. R. Pauw, Y. J. Colón and S. Furukawa, Multiscale structural control of linked metal–organic polyhedra gel by aging-induced linkage-reorganization, *Chem. Sci.*, 2021, **12**, 12556–12563.

34 Z. Wang, G. A. Craig, A. Legrand, F. Haase, S. Minami, K. Urayama and S. Furukawa, Porous Colloidal Hydrogels Formed by Coordination-Driven Self-Assembly of Charged Metal-Organic Polyhedra, *Chem.–Asian J.*, 2021, **16**, 1092–1100.

35 Y. Gu, E. A. Alt, H. Wang, X. Li, A. P. Willard and J. A. Johnson, Photoswitching topology in polymer networks with metal–organic cages as crosslinks, *Nature*, 2018, **560**, 65–69.

36 J. P. Gong, Y. Katsuyama, T. Kurokawa and Y. Osada, Double-Network Hydrogels with Extremely High Mechanical Strength, *Adv. Mater.*, 2003, **15**, 1155–1158.

37 R. Zhu, D. Zhu, Z. Zheng and X. Wang, Tough double network hydrogels with rapid self-reinforcement and low hysteresis based on highly entangled networks, *Nat. Commun.*, 2024, **15**, 1344.

38 S. Mondal, A. J. Wong, M. A. Wagh, L. Alperstein, G. J. Sanjayan and B. S. Sumerlin, Creep resistance in doubly crosslinked dynamic covalent networks, *Polym. Chem.*, 2024, **15**, 1826–1832.

39 M. Zhang, W. Choi, M. Kim, J. Choi, X. Zang, Y. Ren, H. Chen, V. Tsukruk, J. Peng, Y. Liu, D. H. Kim and Z. Lin, Recent Advances in Environmentally Friendly Dual-crosslinking Polymer Networks, *Angew. Chem., Int. Ed.*, 2024, **63**, e202318035.

40 C. P. Kabb, C. S. O'Bryan, C. C. Deng, T. E. Angelini and B. S. Sumerlin, Photoreversible Covalent Hydrogels for Soft-Matter Additive Manufacturing, *ACS Appl. Mater. Interfaces*, 2018, **10**, 16793–16801.

41 A. Carné-Sánchez, J. Albalad, T. Grancha, I. Imaz, J. Juanhuix, P. Larpent, S. Furukawa and D. Maspoch, Postsynthetic Covalent and Coordination Functionalization of Rhodium(II)-Based Metal–Organic Polyhedra, *J. Am. Chem. Soc.*, 2019, **141**, 4094–4102.

42 C. v. Baeckmann, J. Martínez-Esaín, J. A. Suárez del Pino, L. Meng, J. Garcia-Masferrer, J. Faraudo, J. Sort, A. Carné-Sánchez and D. Maspoch, Porous and Meltable Metal–Organic Polyhedra for the Generation and Shaping of Porous Mixed-Matrix Composites, *J. Am. Chem. Soc.*, 2024, **146**, 7159–7164.

43 M. Abdallh, C. Yoshikawa, M. T. W. Hearn, G. P. Simon and K. Saito, Photoreversible Smart Polymers Based on $2\pi + 2\pi$ Cycloaddition Reactions: Nanofilms to Self-Healing Films, *Macromolecules*, 2019, **52**, 2446–2455.

44 J. Ling, M. Z. Rong and M. Q. Zhang, Coumarin imparts repeated photochemical remendability to polyurethane, *J. Mater. Chem.*, 2011, **21**, 18373–18380.

45 H. He, M. Feng, Q. Chen, X. Zhang and H. Zhan, Light-Induced Reversible Self-Assembly of Gold Nanoparticles Surface-Immobilized with Coumarin Ligands, *Angew. Chem., Int. Ed.*, 2016, **55**, 936–940.

46 A. Concellón, P. Romero, M. Marcos, J. Barberá, C. Sánchez-Somolinos, M. Mizobata, T. Ogoshi, J. L. Serrano and J. del Barrio, Coumarin-Containing Pillar[5]arenes as Multifunctional Liquid Crystal Macrocycles, *J. Org. Chem.*, 2020, **85**, 8944–8951.

47 J. Bae, K. Baek, D. Yuan, W. Kim, K. Kim, H.-C. Zhou and J. Park, Reversible photoreduction of Cu(ii)–coumarin metal–organic polyhedra, *Chem. Commun.*, 2017, **53**, 9250–9253.

48 N. J. Oldenhuis, K. P. Qin, S. Wang, H.-Z. Ye, E. A. Alt, A. P. Willard, T. Van Voorhis, S. L. Craig and J. A. Johnson, Photoswitchable Sol–Gel Transitions and Catalysis Mediated by Polymer Networks with Coumarin-Decorated Cu24L24 Metal–Organic Cages as Junctions, *Angew. Chem., Int. Ed.*, 2020, **59**, 2784–2792.

49 K. Gnanaguru, N. Ramasubbu, K. Venkatesan and V. Ramamurthy, A study on the photochemical dimerization of coumarins in the solid state, *J. Org. Chem.*, 1985, **50**, 2337–2346.

50 T. Wolff and H. Görner, Photodimerization of coumarin revisited: Effects of solvent polarity on the triplet reactivity and product pattern, *Phys. Chem. Chem. Phys.*, 2004, **6**, 368–376.

51 S. Inacker, J. Fanelli, S. I. Ivlev and N. A. Hampp, Intramolecular Coumarin-Dimer Containing

Polyurethanes: Optical Tuning via Single- and Two-Photon Absorption Processes, *Macromolecules*, 2022, **55**, 8461–8471.

52 M. Inada, T. Horii, T. Fujie, T. Nakanishi, T. Asahi and K. Saito, Debonding-on-demand adhesives based on photo-reversible cycloaddition reactions, *Mater. Adv.*, 2023, **4**, 1289–1296.

53 M. Y. Tsang, S. Tokuda, P.-C. Han, Z. Wang, A. Legrand, M. Kawano, M. Tsujimoto, Y. Ikeno, K. Urayama, K. C. W. Wu and S. Furukawa, Controlled Sequential Assembly of Metal–Organic Polyhedra into Colloidal Gels with High Chemical Complexity, *Small Struct.*, 2022, **3**, 2100197.

54 Z. Wang, T. Aoyama, E. Sánchez-González, T. Inose, K. Urayama and S. Furukawa, Control of Extrinsic Porosities in Linked Metal–Organic Polyhedra Gels by Imparting Coordination-Driven Self-Assembly with Electrostatic Repulsion, *ACS Appl. Mater. Interfaces*, 2022, **14**, 23660–23668.

55 S. Furukawa, N. Horike, M. Kondo, Y. Hijikata, A. Carné-Sánchez, P. Larpent, N. Louvain, S. Diring, H. Sato, R. Matsuda, R. Kawano and S. Kitagawa, Rhodium–Organic Cuboctahedra as Porous Solids with Strong Binding Sites, *Inorg. Chem.*, 2016, **55**, 10843–10846.

56 J. W. M. Osterrieth, J. Rampersad, D. Madden, N. Rampal, L. Skoric, B. Connolly, M. D. Allendorf, V. Stavila, J. L. Snider, R. Ameloot, J. Marreiros, C. Ania, D. Azevedo, E. Vilarrasa-Garcia, B. F. Santos, X.-H. Bu, Z. Chang, H. Bunzen, N. R. Champness, S. L. Griffin, B. Chen, R.-B. Lin, B. Coasne, S. Cohen, J. C. Moreton, Y. J. Colón, L. Chen, R. Clowes, F.-X. Coudert, Y. Cui, B. Hou, D. M. D'Alessandro, P. W. Doheny, M. Dincă, C. Sun, C. Doonan, M. T. Huxley, J. D. Evans, P. Falcaro, R. Ricco, O. Farha, K. B. Idrees, T. Islamoglu, P. Feng, H. Yang, R. S. Forgan, D. Bara, S. Furukawa, E. Sanchez, J. Gascon, S. Telalović, S. K. Ghosh, S. Mukherjee, M. R. Hill, M. M. Sadiq, P. Horcajada, P. Salcedo-Abraira, K. Kaneko, R. Kukobat, J. Kenvin, S. Keskin, S. Kitagawa, K.-i. Otake, R. P. Lively, S. J. A. DeWitt, P. Llewellyn, B. V. Lotsch, S. T. Emmerling, A. M. Pütz, C. Martí-Gastaldo, N. M. Padial, J. García-Martínez, N. Linares, D. Maspoch, J. A. Suárez del Pino, P. Moghadam, R. Oktavian, R. E. Morris, P. S. Wheatley, J. Navarro, C. Petit, D. Danaci, M. J. Rosseinsky, A. P. Katsoulidis, M. Schröder, X. Han, S. Yang, C. Serre, G. Mouchaham, D. S. Sholl, R. Thyagarajan, D. Siderius, R. Q. Snurr, R. B. Goncalves, S. Telfer, S. J. Lee, V. P. Ting, J. L. Rowlandson, T. Uemura, T. Iiyuka, M. A. van der Veen, D. Rega, V. Van Speybroeck, S. M. J. Rogge, A. Lamaire, K. S. Walton, L. W. Bingel, S. Wuttke, J. Andreo, O. Yaghi, B. Zhang, C. T. Yavuz, T. S. Nguyen, F. Zamora, C. Montoro, H. Zhou, A. Kirchon and D. Fairen-Jimenez, How Reproducible are Surface Areas Calculated from the BET Equation?, *Adv. Mater.*, 2022, **34**, 2201502.

57 K. Leng, H. Sato, Z. Chen, W. Yuan and T. Aida, "Photochemical Surgery" of 1D Metal–Organic Frameworks with a Site-Selective Solubilization/Crystallization Strategy, *J. Am. Chem. Soc.*, 2023, **145**, 23416–23421.

58 F. Zeng, Z. Fan, S. Wu, X. Cheng and Y. Tian, Photo-patterned oxygen sensing films based on Pt porphyrin for controlling cell growth and studying metabolism, *RSC Adv.*, 2019, **9**, 924–930.